Accepted Manuscript

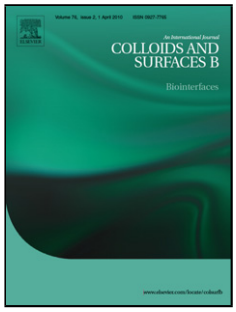

Title: Effect of energy source, salt concentration and loading force on colloidal interactions between *Acidithiobacillus ferrooxidans* cells and mineral surfaces

Author: Mengxue Diao Tuan A.H. Nguyen Elena Taran Stephen Mahler Anh V. Nguyen

PII: S0927-7765(15)00324-0
DOI: http://dx.doi.org/doi:10.1016/j.colsurfb.2015.05.026
Reference: COLSUB 7099

To appear in: *Colloids and Surfaces B: Biointerfaces*

Received date: 7-3-2015
Revised date: 11-5-2015
Accepted date: 14-5-2015

Please cite this article as: M. Diao, T.A.H. Nguyen, E. Taran, S. Mahler, A.V. Nguyen, Effect of energy source, salt concentration and loading force on colloidal interactions between *Acidithiobacillus ferrooxidans* cells and mineral surfaces, *Colloids and Surfaces B: Biointerfaces* (2015), http://dx.doi.org/10.1016/j.colsurfb.2015.05.026

Highlights:

- Distinct retraction patterns of *A. f* grown with different energy sources were observed
- Interaction forces between *A. f* and minerals with bacterial probe were quantified
- The conformation of surface biopolymers was affected by salt concentration

GRAPHICAL ABSTRACT

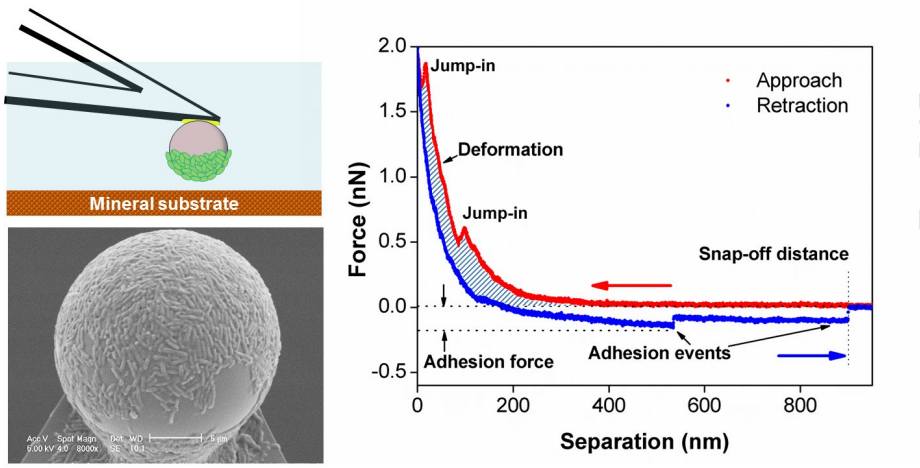

A bacterial colloid probe and representative force-separation curves

Effect of energy source, salt concentration and loading force on colloidal interactions between *Acidithiobacillus ferrooxidans* cells and mineral surfaces

Mengxue Diao[1,¶], Tuan AH Nguyen[1], Elena Taran[2], Stephen Mahler[1, 2], Anh V. Nguyen[1*]

[1]School of Chemical Engineering

The University of Queensland, Brisbane, Queensland 4072, Australia

[2]ANFF-Q, The University of Queensland, Brisbane, Queensland 4072, Australia

[¶] Current Address: Scientific Research Academy of Guangxi Environmental Protection, Nanning, Guangxi 530022, China

[*]Corresponding Author: Phone +61-7-33653665, Email: anh.nguyen@eng.uq.edu.au

Statistical summary of manuscript

Total number of words: 5986

Number of Figures: 7

Number of Tables: 1

Abstract

The surface appendages and extracellular polymeric substances of cells play an important role in the bacterial adhesion process. In this work, colloidal forces and nanomechanical properties of *Acidithiobacillus ferrooxidans* (*A. f*) interacted with silicon wafer and pyrite (FeS_2) surfaces in solutions of varying salt concentrations were quantitatively examined using the bacterial probe technique with atomic force microscopy. *A. f* cells were cultured with either ferrous sulfate or elemental sulfur as key energy sources. Our results show that *A. f* cells grown with ferrous ion and elemental sulfur exhibit distinctive retraction force vs separation distance curves with stairstep and sawtooth shapes, respectively. During the approach of bacterial probes to the substrate surfaces, surface appendages and biopolymers of cells are sequentially compressed. The conformations of surface appendages and biopolymers are significantly influenced by the salt concentrations.

Keywords: Atomic force microscopy, *Acidithiobacillus ferrooxidans*, bacterial adhesion, nanomechanical properties

1. Introduction

Bacterial adhesion to mineral surfaces is of great importance to the growth of bacteria in natural habitats and many industrial applications [1, 2]. In these processes, the bacterial surface largely determines the adhesion process by the surface appendages (*e.g.* pili and flagella) and extracellular polymeric substances. In the bioleaching process, *Acidithiobacillus ferrooxidans* (*A. f)* was the first described metal sulfide oxidizing microorganism, which is affiliated with the Gram-negative γ-Proteobacteria. It is one of the most important species in the bioleaching of sulfide ores operating at temperature lower than 40 °C [3]. *A. f* is endowed

with a remarkably broad metabolic capacity, as it can live on the oxidation of ferrous salts, elemental sulfur and a variety of sulfide minerals [4][5, 6].

Various growth substrates may induce physiological differences in the chemical composition of cell surfaces, which reflects the response of cells in optimizing nutrient uptake. Research associated with macroscopic assays of bacterial adhesion [7, 8], analysis of chemical compositions for cell surface biopolymers [8, 9], and characterization of cell surface structures [10, 11] has been well documented in the literature. However, the effect of different energy sources on bacterial adhesion behavior and the correlation between surface properties and fundamental interacting forces have not been fully resolved at nanoscale.

In the past decade, remarkable developments in atomic force microscopy (AFM) have made it a versatile tool to determine the surface structures and specific interactions of biological samples under near-physiological conditions [12, 13]. AFM is capable of sensing picoNewton forces in aqueous solutions, and the obtained force-separation curves can provide information on the adhesive and nanomechanical properties of biological samples [14-18]. Tipped cantilevers have been extensively used as indenters to probe the elastic properties of different bacterial cells such as *Escherichia coli* [19, 20], *Pseudomonas aeruginosa* [21] and *Shewanella putrefaciens* [18]. Alternatively, a cell probe [20, 22] can be used to measure the overall mechanical properties of the cell. A colloidal probe (a microsphere glued onto the end of a cantilever) is often used to indent larger mammal cells [17, 23]. However, the use of AFM to investigate the nanomechanical properties of bioleaching bacteria has been rarely reported.

The goal of this study is to relate the adhesion behavior and nanomechanical interactions to the biophysical responses of bacterial cells to the change of environmental conditions (energy sources and salt concentrations). To this end, we performed AFM force

measurements using bacterial probes constructed with *A. f* cells grown with different energy sources of Fe^{2+} and S^0, and exposed the bacterial probes to solutions of various salt concentrations. The shape of the retraction curves, adhesion forces and the Young's moduli of cell surface biopolymers were compared for *A. f* cells grown in different energy sources. Interesting features such as sequential "jump-in" events of approaching curves and distinct retraction curve patterns of *A. f* cells grown with the energy sources were obtained. Overall, our findings quantitatively describe the adhesion behaviors of *A. f* on mineral surfaces and the nanomechanical properties may help the further understanding of responses of cell surface appendages to environmental stimuli.

2. Materials and methods

2.1 Microorganism and growth conditions

A. f was kindly provided by Professor Guohua Gu (School of Mineral Processing and Bioengineering, Central South University, China). Cells were cultured at 30 °C in 9K medium (pH 2.0) [24]: $(NH_4)_2SO_4$ 3 g/L, KCl 0.1 g/L, $K_2HPO_4{\cdot}3H_2O$ 0.5 g/L, $MgSO_4{\cdot}7H_2O$ 0.5 g/L, $Ca(NO_3)_2$ 0.01 g/L. Bacteria were grown with 4.47% (w/v) $FeSO_4$ and 3% (w/v) elemental sulfur as energy source, respectively. *A. f* cells were incubated on a rotary shaker at 170 rpm to their mid-exponential growth phase.

2.2 Substrate preparation

The silicon wafers (100 oriented with a 100-nm thermal-oxide surface layer) were purchased from Silicon Valley Microelectronics (USA). The silica surfaces were cleaned using the RCA SC-1 process [25] and stored in Milli-Q deionized water (18.2 MΩcm, Millipore, USA) before use. A museum-grade pyrite (FeS_2) sample obtained from Ward's Natural Science was embedded in an epoxy resin and cut off in a thickness of 3 mm. The sample slice was manually polished with 3 μm and 1 μm diamond suspensions, respectively,

and thoroughly washed with acetone, ethanol and copious amount of deionized water. The sample slice was UV treated for 30 min before exposure to the bacterial probe.

2.3 Zeta potential measurements

Cultures in the mid-exponential phase were filtered through Whatman filter paper to remove suspended solid materials. Cells were harvested by centrifugation at acceleration of 10000 g-units for 15 min. The cell pellet was washed three times using sterilized H_2SO_4 (pH 1.5) and deionized water to remove trapped ions. The washed cell pellet was re-suspended in 0.001, 0.01, 0.1 and 1 M KCl solutions, respectively, to obtain a concentration of approximately 1×10^7 cells/mL. The zeta potentials of *A. f* were measured using a zeta potential analyzer (ZetaPLUS analyzer, Brookhaven Instruments Corp.) and calculated from the electrophoretic mobility using the Smoluchowski equation embedded in the ZetaPlus software. Measurements were conducted in triplets and the average value was used.

The zeta potential of planar silica surfaces was obtained using an EKA (electro kinetic analyzer) with an asymmetric clamping cell (Anton Paar, GmbH, Austria). A piece of PMMA was used as a supporting medium (back-plate) in the asymmetric clamping cell. The streaming potential measurements were taken three times in each salt solution. The zeta potential was calculated from the streaming potential according to the approach developed by Fairbrother and Mastin embedded in the software [26]. The isoelectric point of pyrite surface was reported to be about pH 2 in literatures [27].

2.4 ATR FT-IR spectroscopy

Cells in the mid-exponential phase were collected and washed three times with H_2SO_4 and deionized water. Cell pellets were dried at 50 °C for 30 min before acquiring the spectra.

The infrared spectra of bacterial surfaces were measured using a Perkin Elmer Spectrum 100 spectrometer. Spectra were the results of 43 scans with a resolution of 1 cm^{-1} in the range 650-4000 cm^{-1}.

2.5 Preparation of bacterial probes

Bacterial probes were prepared using a protocol described in the previous study [28]: Tipless cantilevers (Veeco, model NP-OW) were cleaned with strong oxidizing Piranha solution [29] for 30 min, and rinsed with copious amounts of deionized water before blow-drying with high purity compressed nitrogen gas. A silica microsphere (20 μm in diameter, Fuso Chemical Co., Japan) cleaned by the RCA SC-1 solution was glued to the end of a tipless cantilever with a small amount of thermoplastic epoxy resin using a micromanipulator under an optical microscope. The colloidal probe was functionalized with 1% (w/v) polyethyleneimine (PEI, MW~1300, Sigma-Aldrich, Australia) solution for 2.5 h. The excess solution was decanted and the probe was rinsed in deionized water and stored at 4 °C.

Bacterial pellets were washed and resuspended in a 3% (v/v) glutaraldehyde solution for cell fixation at 4 °C for 2.5 h [30]. After fixation the cells were washed with phosphate buffer solution (PBS), and resuspended in PBS at 4 °C overnight. The cell suspension was spread onto a clean glass slide to allow the colloidal probe to touch the suspension by the means of a micromanipulator. The bacterial probe was then gently rinsed with deionized water to remove loosely attached cells and kept hydrated before force measurements. Scanning electron microscopy (SEM) (Philips XL-30) was performed on all bacterial probes after AFM measurements to verify the presence of cells on the microsphere.

142 **2.6 AFM force measurements**

143 Ultrahigh purity KCl (Sigma-Aldrich) was roasted at 500 °C for 12 h and used as the
144 supporting electrolyte. Force measurements were performed at room temperature in KCl
145 solutions at natural pH 5.6±0.5 using a MFP-3D atomic force microscope (Asylum Research,
146 Santa Barbara, CA) equipped with a closed fluid cell. The actual spring constants of the
147 cantilevers were determined using the thermal noise method embedded in the Asylum
148 Research AFM software [31]. The cantilevers used in this study were found to have a spring
149 constant of 0.09±0.02 N/m. After each probe being immersed in the solution for at least 20
150 min, force curves were recorded under a loading force of 2 nN at an approaching/retraction
151 velocity of 500 nm/s with a piezo movement of 6000 nm. At least three probes, as well as the
152 control probe (PEI-coated silica colloid probe), were used for each set of experiments at 3-5
153 contact locations per probe.

154 To investigate the effect of loading force on the nanomechanical properties of bacterial
155 cells, the force curves were measured at different loading forces from 0.5 nN to 2.8 nN. After
156 a series of consecutive force measurements applying increasing loading forces, the
157 measurement was conducted again at 2 nN. Once this force profile differed from the
158 previously measured ones at 2 nN, the bacterial probe was considered damaged and replaced
159 by a new one.

2.7 AFM data analysis

2.7.1 Raw data conversion

From the approaching and retraction curves, several useful parameters can be extracted, for instance, the adhesion force, snap-off distance and Young's modulus. Due to the deformable nature of biological samples, a correct conversion from raw data to the force-separation curves is crucial to the investigation of bacteria-mineral interactions.

The direct results (raw data) recorded by AFM in a force measurement is a measure of the cantilever deflection (d, V) versus the relative piezo displacement (z, nm). Deflection (V) can be converted to cantilever deflection (nm) with a sensitivity of the cantilever obtained by engaging the cantilever against a rigid surface. The raw data can then be converted to force (nN or pN) according to Hooke's law: $F = k_c d$, where k_c is the spring constant of the cantilever. For deformable bacterial cells, the conversion from raw data to force-separation curves is not as simple as that for rigid solid surfaces. The cell deforms in response to the interaction forces and loading forces as shown in Fig. 1A. When the bacterial probe is brought toward the substrate surface, the soft cell is squeezed, reflecting the deformation of the cell surface appendages, biopolymer brush and/or the cell body depending on the magnitude of loading force.

The distance balance, $z_0 + 2R + s_0 = (z - d) + 2R + (s - \delta)$, gives the following equation for the actual separation distance s:

$$s = (z_0 + s_0) + \delta + d - z \quad (1)$$

The relative piezo position z and the cantilever deflection d are directly obtained from the AFM measurement, while the values of sample deformation δ and $z_0 + s_0$ have to be determined. Due to the deformable nature of cells and the presence of interaction forces

between cells and the substrate surfaces, we fit the portion of raw data at high loading force with the Hertz model to determine the required parameters (see Section 2.7.3 for more detail).

2.7.2 Steric model

Cell surface appendages and/or biopolymer chains can be considered as a layer of polymeric brush. The steric forces are often the dominant forces during the approach of cells to solid surfaces, particularly in high ionic strength solutions where the electrostatic forces between cell and substrate surfaces are largely compressed. The steric force per unit area between two surfaces, only one of which is coated with polymers is estimated by [32, 33]

$$f = 50 k_B T \Gamma^{3/2} e^{-2\pi s/L_0} \tag{2}$$

where k_B is the Boltzmann constant, T is the absolute temperature, s is the distance between the two surfaces, Γ is the density of grafted polymers in m^{-2} and L_0 is equilibrium length of the polymer brush.

In our case, the substrate surface is bare, while the cell surface is covered with biopolymers and considered as a microsphere with a radius R of 500 nm (Fig. 1B). We approximate the total force by integrating f over half of the cell surface as follows:

$$F = \int_0^{\frac{\pi}{2}} f 2\pi r dr = \int_0^{\frac{\pi}{2}} f 2\pi R^2 \sin\theta d\theta = 50 k_B T R \Gamma^{3/2} L_0 e^{-2\pi(s+R)/L_0} \left(1 - e^{-2\pi R/L_0}\right) \tag{3}$$

where $r = R\sin\theta$ is the radial distance from a random point on the cell surface to the vertical axis of symmetry.

2.7.3 Hertz model

Among different models describing the elastic response of soft samples, the Hertz model has been widely used to describe similar systems in AFM experiments [17, 34-36]. In the Hertz theory, the cell is assumed to be an isotropic material with a well-defined interface and

any surface interactions or adhesions are neglected [37]. At the region of Hertz contact, we have the following equations for the distance of cell deformation and the force of cell deformation in contact with a rigid plane to the AFM data [38]:

$$\delta = Ad^{2/3} \tag{4}$$

$$F = \frac{4}{3}\frac{E}{1-\nu^2}R^{1/2}\delta^{3/2} \tag{5}$$

where E is the Young's modulus, R is the radius of bacterial cells, taken as 500 nm, ν is the Poisson's ratio of the deformable bacterial cells (assumed to be 0.5) [34] and A represents relationships between the sample radius, the Poisson ratio and the Young's modulus of the sample according to different geometries of the systems. The Young's modulus of a bacterial cell is obtained from quantitative interpretation of the non-linear regime that follows the steric interaction portion.

The deformation δ is dependent on the contact point of the bacterial probe with the substrate. However, due to the influence of interaction forces (*e.g.* steric repulsion), it is difficult to determine the accurate contact point. Various approaches such as manual determination by visual inspection [36], semi-automated [39, 40] and automated approach with software [41, 42], have been used for determining the contact point. Here, we fit the region of raw curve at high loading force with the Hertz model to determine the separation between bacteria and substrate surfaces and the Young's modulus of the cell with Eq. (1) and (5).

2.7.4 WLC model

The wormlike chain (WLC) model is commonly used to describe the elasticity of the biopolymer chains such as proteins and DNA [43-45]:

$$F(s) = \frac{k_B T}{L_p}\left[\frac{s}{L_c} + \frac{1}{4(1 - s/L_c)^2} - \frac{1}{4}\right] \quad (6)$$

where L_p and L_c are the persistence length and contour length of the polymer chains. In this study, the WLC model was applied to interpret the sawtooth-shaped adhesion events of sulfur-grown cells.

3. Results and discussion

3.1 Bacterial probes

The SEM image in Fig. 2A shows a cell-coated colloidal probe which was used for a series of force measurements. The contact area of the microsphere was covered by bacterial cells, thus the measured force curves can reflect the true bacterial-mineral interactions. Fig. 2C displays typical approach and retraction force curves recorded from a ferrous ion-grown cell probe. Far from the substrate surface, the bacterial probe senses no interaction forces between the surfaces. As the probe approaches the substrate, the approaching curve exhibits a repulsive force with several jump-in events. After the mutual contact, adhesins of cells adhere to the substrate surface and show multiple adhesion events during retraction. The deviation in the contact region between the approaching and retraction part of the force curve (the shaded area) is due to the deformation of the cell. Usually, the typical "loading-unloading hysteresis" can help to verify the quality of bacterial probes before conducting SEM tests.

3.2 Surface characterization

The zeta potentials of ferrous ion- and sulfur-grown *A. f* and the silica wafer in the presence of various salt concentrations are shown in Fig. 3A. At neutral pH, bacterial cells are negatively charged and the absolute value of zeta potential decreases with an increase of the salt concentration, which is in line with enhanced screening of the charges within the

surface appendage and/or biopolymer chains by ions present in the solution. The ferrous ion-grown cells were slightly more negatively charged than sulfur-grown cells in all solutions, which is in agreement with the findings of Sharma *et al.* [46]. The zeta potential results demonstrate that different energy sources can affect the surface charge of *A. f*.

An early study [47] found that *A. f* cells cultured with sulfur, pyrite (FeS_2) and chalcopyrite ($CuFeS_2$) are more hydrophobic than ferrous ion-grown cells, indicating that various energy sources can affect the cell surface properties. The depletion of soluble ferrous salts renders the bacteria prone to attaching to the solid energy source such as elemental sulfur and sulfide minerals for growth, which results in the synthesis of more proteinaceous substances for the purpose of facilitating adhesion [8, 9, 46]. To analyze the difference of functional groups on cell surfaces induced by various energy sources, ATR-FTIR tests were performed.

As can be seen in Fig. 3B, most peaks in the spectra of ferrous ion- and sulfur-grown cells are at similar positions. The assignments of the peaks indicate that *A. f* surface consists of extracellular polysaccharides, proteins and nucleic acids [48, 49]. Previous FTIR results reported by Devasia et al. [47] suggested that a proteinaceous new cell surface appendage was synthesized in sulfur-grown cells while such an appendage was found to be absent in ferrous ion-grown cells. Our FTIR results differ from their results because cells cultured with either ferrous ion or elemental sulfur show similar peaks which represent the proteins. The only remarkable difference is in the range of 1345~1403 cm^{-1}. Ferrous ion-grown cells show a small peak at 1388 cm^{-1} which is absent in the sulfur-grown ones. Sulfur-grown *A. f* possess two peaks at 1403 and 1345 cm^{-1} respectively, which are absent in the spectra of ferrous ion-grown cells. The peaks in the range of 1388~1403 cm^{-1} represent the C=O symmetric stretching of COO- group in amino acids and fatty acids. The weak peak at 1345 cm^{-1} represents sulfonic acid. Interestingly, the peak at 1388 cm^{-1} was observed in the FTIR

spectra of *L. ferrooxidans*, which is also a ferrous ion-oxidizer, while the peak at 1403 cm^{-1} was observed in the spectra of *A. thiooxidans* which is a sulfur oxidizer [28]. It can be inferred from the qualitative FTIR data that specific energy sources can likely induce the differential expression of specific extracellular biopolymers and lead to the difference in the ratio of various biopolymers.

3.3 Analysis of retraction curves

The retraction curves were examined to obtain information regarding the adhesion behavior (*i.e.* adhesion force and snap-off distance) of the bacterial cells. Representative force-separation curves recorded between *A. f* cells and substrates are shown in Fig. 4. A notable proportion of the retraction curves obtained from ferrous ion-cultured cells are characterized by a stair-step separation, while those recorded from sulfur-cultured cells are featured by larger adhesion forces with sawtooth-shaped multiple peaks. Both separation patterns indicate that the molecular bonds formed between bacterial cells and the substrate surfaces break sequentially until they completely separated from each other [15].

A possible reason for the distinct retraction patterns is the energy source-induced differential expression of biopolymers. The stair-step separation pattern likely results from the extension or desorption of extracellular polysaccharides, which was reported by Sletmoen *et al.* [50]. The sawtooth shaped adhesion peaks, which can be well fitted with WLC model, are typical for the stretching of proteins. The fraction of the extracellular proteins of *A. f* cultured with ferrous ion and sulfur was examined by chemical analysis [8] and two-dimensional gel electrophoresis [51]. The results reveal higher amount of protein on sulfur-grown cells compared to ferrous ion-grown cells and the various ratios of total polysaccharides to proteins are responsible for the different attachment abilities of *A. f*, which is also in line with our AFM measurements.

As expected for biological samples, the shape of each retraction curve, the number of adhesion events, the magnitude of adhesion forces and the snap-off distances vary from retraction to retraction (Fig. 4 and Table 1). This is attributed to the heterogeneity of the bacterial surface. Different types of biopolymers exist on the cell surface and more than one type can randomly adhere to the substrate surface on contact. In addition, a biopolymer chain can adhere to the substrate at multiple sites on the chain.

The properties of retraction curves are summarized in Table 1. To determine the statistical significance of the adhesiveness differences between ferrous ion- and sulfur-grown *A. f*, we plotted the adhesion forces in histograms (Fig. 4). The data display more than 800 retraction curves in total obtained from at least three independent experiments using different bacterial probes and substrates under each salt concentration. As shown in Fig. 4, a wide distribution of adhesion forces was observed due to the heterogeneous nature of the bacterial surface. Salt concentration did not dramatically affect the mean adhesion forces of ferrous ion- or sulfur-grown *A. f*. The adhesion forces of ferrous ion-grown cells are similar to that of sulfur-grown cells on the pyrite surface. Comparing with other sets of experiments, sulfur-grown *A. f* exhibits a higher adhesion affinity to the silica surface. It is interesting to note that, the stair-step unfolding force of ferrous ion-grown cells increases with an increase of the salt concentration, which indicates that biopolymers become stiffer in solutions of higher salt concentration and require larger unfolding forces during retraction.

A wide range of the snap-off distances between the bacterial probe and the substrate surfaces was also observed in all solutions (Fig. 5), which again reflects the heterogeneity of the biopolymers on the bacterial surface. The various snap-off distances also provide solid evidence of different responses of the surface appendages and biopolymer chains to various salt concentrations. The snap-off distances vary in a wide range up to 2.2 μm, demonstrating the existence of pili and/or flagella. However, due to the use of different bacterial probes and

the small number of flagella, the frequency of the flagella adhesion events (larger than 1μm) is low.

3.4 Analysis of approaching curves

The size of the biopolymers/surface appendages is sufficient to cause the steric repulsion between the bacterial probe and the substrate surface. When the bacterial probes are gradually lowered to touch the substrate surfaces, the steric interactions between the substrate and cell surface biopolymers are first sensed by the probes, followed by mechanical contact and deformation of the surface appendages and polymer brush of the cell envelope as a result of the compression. The physical properties such as the net surface charge of cells and minerals and the conformation of biopolymers change with increasing the salt concentration.

In this study, the steric model and Hertz model were applied to the force curves to estimate the length and Young's modulus of the biopolymer layer. Although the electrical double layer force can also demonstrate exponential repulsive behavior, the electrostatic interaction at high salt concentration was weak and ignored because the spatial range where the steric repulsions are operative is significantly larger than that of the electrostatic forces. The Decay length in 0.001 M KCl is approximately 9.7 nm, while the repulsion starts from approximately 600 nm (Fig. 6A). This suggests that the electrostatic model is not applicable to these biopolymers, thus it is justified only to use the steric model and Hertz model to interpret the approaching curves. For approach curves analysis, we only consider the force curves between bacterial probes and the silica wafer, which is more homogeneous and smoother than the pyrite surface.

3.4.1 Effect of salt concentration on biopolymer

A significant effect of salt concentration on the approaching curves was observed (Fig. 6A and B). The steric model (Eq. (3)) was fitted to the approaching curves at various salt

concentrations. For ferrous ion-grown *A. f*, the distance of the repulsion force decreased with an increase of the salt concentration (Fig. 6A). From 0.001 M to 1 M salt concentration, the equilibrium length of the polymer brush L_0 was 675±60, 415±23, 383±21 and 236±4 nm, respectively. The grafted polymer density Γ was between 6.9×10^{16} m^{-2} to 13.9×10^{16} m^{-2}, the magnitude of which was in agreement with other reports [2, 35, 52]. It is interesting to note that the sulfur-grown cells showed an opposite trend. As can be seen from Fig. 6B, the approaching curves of sulfur-grown *A. f* showed more repulsive peaks and the distance of repulsion gradually increased with an increase of the salt concentration.

The histograms presented in Fig. 6C and D were obtained by analyzing more than 50 approaching curves using Eq. 5 for each salt concentration, resulting in different Young's modulus distributions. In our experiments, the applied forces (2 nN) were only sufficient to indent less than 200 nm even in 0.001 M KCl solution (smaller than polymer brush thickness estimated by the steric model). This indicates that the applied forces were mainly used to compress the outer biopolymer brush of the cell wall.

Generally, the average values of Young's modulus of ferrous ion-grown cells are larger than that of the sulfur-grown cells in all solutions. The Young's modulus of ferrous ion-grown *A. f* increased with increasing salt concentration. From 0.001 M to 1 M solution, the average value of E was 30.2±8.9, 29.2±5.1, 46.5±5.1 and 64.5±9.1 kPa, respectively. The Young's moduli of sulfur-grown *A. f* were similar (about 22 kPa) at 0.001 M and 0.01 M KCl. However, the peak distribution of E shifted toward smaller values as the salt concentration increased, showing 14.9±7.1 and 17.2±9.4 kPa at 0.1 M and 1 M, respectively. The Young's moduli obtained from our experimental data by interpretation with Hertz model are in agreement with the magnitudes reported in the literature for E of bacterial biopolymer layers [19, 22, 35, 53], generally ranging from 1 to 100 kPa.

In salt solutions with neutral pH, bacterial cells and substrate surface are negatively charged due to the presence of anionic groups such as carboxyl and phosphate groups. By increasing the salt concentration of the solution, the repulsive interactions between neighboring charged chains of biopolymer are screened, leading to the collapse of the biopolymer chains onto the cell membrane [54]. In low salt concentration solutions, the biopolymer chains are more extended (larger L_0), resulting in softer bacterial cells (smaller E). However, the biopolymer thickness of sulfur-grown cells increased with increasing salt concentration. The E value of sulfur-grown cells is approximately 4 times softer than that determined for ferrous ion-grown cells at 1 M. Although the reasons for the opposite trend observed from sulfur-grown cells are as yet not well understood, the results seem to agree with the surface characterization results and indicate that the presence of different external polymeric appendages and/or biopolymers and the change in the ratio between different biopolymers lead to the varied nanomechanical properties of *A. f*. Other surface-specific equipment such as sum frequency generation may be helpful to reveal the molecular differences in surface biopolymers on the cell surface in further researches.

The absolute determination of the Young's modulus for a biological sample may not be accurate for the following reasons: (a) *A. f* cells are rod-shaped instead of a spherical shape. (b) The simple Hertz model ignores the cell-substrate adhesion. (c) The homogeneous assumption for the cell surface in the Hertz model is not physically realistic. The componential and structural complexity in the bacterial surface can lead to variation of the Young's modulus depending on different indentation depth, *i.e.* depending on the layer which is actually squeezed. Various surface components and appendages such as fimbria, flagellum, pili and biopolymer chains can contribute to the overall stiffness measured with AFM. However, a trend in the change of Young's modulus as a function of salt concentration may provide some fundamental information for bacteria-mineral interactions.

3.4.2 Effect of loading force

Upon approaching, the bacterial probe senses a repulsive force due to the steric interaction. A notable fraction of approaching curves exhibit non-monotonic discontinuities referred as sequential "jump-in" events, which reflect large changes in loading force over very small distances. We propose that as the loading force increases, the resistance levied by the surface appendages (pili or flagella) and/or biopolymer chains of cells against the substrate is suddenly relieved, allowing further compression of the cell with less applied force. However, "jump-in" events are rarely observed for experiments between a tip cantilever and bacterial cells in previous studies [2, 52, 55-57].

The reasons for using a colloidal bacterial probe instead of using a tip cantilever as an indenter onto the cell surface are as follows: (a) A sharp tip of the cantilever can possibly penetrate between the biopolymer chains, and deform the cell membrane with the tip apex while deforming a small amount of the polymer chains with the tip sides [17]. (b) A sharp tip with a small contact area can interact with various biopolymers during each approaching process, thus largely enhancing the heterogeneity of the results. To obtain a global nanomechanical property of the cell, a bacterial colloidal probe can provide a much larger contact area, the results from which are equivalent to the average of many measurements with the sharp tip (*i.e.* conducting a nanomechanical force mapping experiment).

The effect of loading force on the approaching curves is illustrated for the interactions between ferrous ion-grown *A. f* and the silica surface in 0.001 M KCl solution. For the sake of illustration, the approaching curves were plotted as loading force versus arbitrary separation. As shown in Fig. 7, under a very small loading force of 0.5 nN, the approaching curve displays a monotonic repulsion due to the steric interaction. As the loading force increases, the approaching curves show a first "jump-in" event at a similar distance around 150 nm. Under higher loading forces, the approaching curves show several smaller "jump-in"

421 events following the first one. Although the number of "jump-in" events generally increases
422 with an increase of the loading force, the number also varies from curve to curve, which
423 again points to the heterogeneities and complexity of cell surfaces. These "jump-in" events
424 likely reflect the sequential compression of the cell surface appendages and biopolymer
425 chains. By fitting the "jump-in" events to the Hertz model, we obtained the *E* values from
426 low to high loading forces are 6.9, 9.0, 18.4, 26.9, 34.8 and 34.5 kPa, respectively. As we can
427 see in Fig. 7, under a loading force larger than 1.5 nN, the Young's moduli of the first
428 compression events are similar and close to the average value of 30.2±8.9 kPa in 0.001 M
429 KCl solution.

430 In order to further rule out the possibility that the "jump-in" events result from the
431 compression of different cells, we used the representative curves in Fig. 7 as an example to
432 estimate the contact area of the bacterial probe. The Hertz contact area can be estimated as
433 follows:

434 $$S = \pi a^2 = \pi \left[\frac{3FR(1-\gamma^2)}{4E} \right]^{2/3} \quad (7)$$

435 As the loading force increases from 0.5 to 2.8 nN, the estimated contact area increases from
436 0.23 to 0.25 μm^2, which is about half of the area of *A. f* cell (*ca.* 0.5 μm^2). Similar results
437 were reported by Zhang et al. [20] that under a loading force of 1.5±0.2 nN, the contact
438 radius of *E. coli* cells is approximately 45±2 nm. Our previous results showed that when the
439 bacterial probe was pressed extremely hard onto the silica surface, the area of destroyed cell
440 layer contained about 10 cells (data not shown). Therefore, under a loading force of 2 nN, it
441 is likely that only one cell is in contact with the substrate, which in turn supports our claim
442 that the sequential compression events reflect the compression of biopolymer chains with
443 different lengths instead of the compression of several cells. Furthermore, we observed that

444 most "jump-in" events of the approaching curves correspond one-to-one with the adhesion
445 peaks of the corresponding retraction curves for sulfur-grown cells. This also indicates the
446 "jump-in" events reflect the compression of fibrous biopolymers.

447 **4. Conclusions**

448 In this study, the fundamental interaction forces between *A. f* cells cultured with different
449 energy sources and the substrates were directly quantified with the bacterial probe technique.
450 Our results show that the conformational changes in biopolymers due to the salt
451 concentration are important factors in influencing the surface potentials, adhesion behavior
452 and the softness of the bacterial cells. This research provides fundamental understanding and
453 evidence that different energy sources and the salt concentration significantly influence the
454 adhesion behavior and cell nanomechanical properties.

455 Bacterial probe technique of AFM is advantageous in direct measurement of the
456 interacting forces between cells and the mineral surface, and is of great importance in the
457 investigation of bacteria-mineral interface research. However, due to a lengthy manual
458 analysis, one often had to compromise by reducing the number of force curves to lower
459 analysis time. For deformable samples with heterogeneous surface components, converting
460 raw data, calculating Young's modulus, and extracting adhesion force and snap-off distance,
461 would have made the manual route very tedious. Commercial data analysis software suitable
462 for batched AFM data analysis of different geometrical systems will be beneficial for faster
463 and more accurate analysis of AFM data in future researches.

464 **Acknowledgements**

465 The authors gratefully acknowledge The University of Queensland Postgraduate
466 Scholarship (UQRS). We thank Mr. Guozhao Ji for advice on the data processing.

References

[1] D. Santhiya, S. Subramanian, K.A. Natarajan, K. Hanumantha Rao, K.S.E. Forssberg, Bio-modulation of galena and sphalerite surfaces using *Thiobacillus thiooxidans*, International Journal of Mineral Processing, 62 (2001) 121-141.

[2] M.N. Chandraprabha, P. Somasundaran, K.A. Natarajan, Modeling and analysis of nanoscale interaction forces between *Acidithiobacillus ferrooxidans* and AFM tip, Colloids and Surfaces B: Biointerfaces, 75 (2010) 310-318.

[3] D.P. Kelly, A.P. Wood, Reclassification of some species of *Thiobacillus* to the newly designated genera *Acidithiobacillus* gen. nov., *Halothiobacillus* gen. nov and *Thermithiobacillus* gen. nov., International Journal of Systematic and Evolutionary Microbiology, 50 (2000) 511-516.

[4] T. Rohwerder, T. Gehrke, K. Kinzler, W. Sand, Bioleaching review part A: Progress in bioleaching: fundamentals and mechanisms of bacterial metal sulfide oxidation, Applied Microbiology Biotechnology, 63 (2003) 239 - 248.

[5] M. Rodriguez-Leiva, H. Tributsch, Morphology of bacterial leaching patterns by *Thiobacillus ferrooxidans* on synthetic pyrite, Archives of Microbiology, 149 (1988) 401-405.

[6] K.J. Edwards, B. Hu, R.J. Hamers, J.F. Banfield, A new look at microbial leaching patterns on sulfide minerals, FEMS Microbiol. Ecol., 34 (2001) 197-206.

[7] A. Vilinska, R.K. Hanumantha, Surface thermodynamics and extended DLVO theory of *Acidithiobacillus ferrooxidans* cells adhesion on pyrite and chalcopyrite, The Open Colloid Science Journal, 2 (2009) 1-14.

[8] L. Xia, Z. Shen, T. Vargas, W. Sun, R. Ruan, Z. Xie, G. Qiu, Attachment of *Acidithiobacillus ferrooxidans* onto different solid substrates and fitting through Langmuir and Freundlich equations, Biotechnol Lett, (2013) 1-8.

[9] T. Gehrke, J. Telegdi, D. Thierry, W. Sand, Importance of extracellular polymeric substances from *Thiobacillus ferrooxidans* for bioleaching, Appl Environ Microb, 64 (1998) 2743 - 2747.

[10] A.A. DISpirito, M. Silver, L. Voss, O.H. Tuovinen, Flagella and pili of iron-oxidizing *Thiobacilli* isolated from a uranium mine in northern Ontario, Canada, Appl. Environ. Microbiol., 43 (1982) 1196-1200.

[11] Y.-Q. Li, D.-S. Wan, S.-S. Huang, F.-F. Leng, L. Yan, Y.-Q. Ni, H.-Y. Li, Type IV pili of *Acidithiobacillus ferrooxidans* are necessary for sliding, twitching motility, and adherence, Curr Microbiol, 60 (2010) 17-24.

[12] T. Cao, A. Wang, X. Liang, H. Tang, G.W. Auner, S.O. Salley, K.Y.S. Ng, Investigation of spacer length effect on immobilized *Escherichia coli* pili-antibody molecular recognition by AFM, Biotechnol Bioeng, 98 (2007) 1109-1122.

[13] L.S. Dorobantu, M.R. Gray, Application of atomic force microscopy in bacterial research, Scanning, (2010) 74-96.

[14] W. Zhang, J. Hughes, Y. Chen, Impacts of hematite nanoparticle exposure on biomechanical, adhesive, and surface electrical properties of *Escherichia coli* Cells, Appl Environ Microb, 78 (2012) 3905-3915.

[15] D. Alsteens, P. Van Dijck, P.N. Lipke, Y.F. Dufrêne, Quantifying the forces driving cell–cell adhesion in a fungal pathogen, Langmuir, (2013).

[16] Y.F. Dufrene, A.E. Pelling, Force nanoscopy of cell mechanics and cell adhesion, Nanoscale, 5 (2013) 4094-4104.

[17] I. Sokolov, M.E. Dokukin, N.V. Guz, Method for quantitative measurements of the elastic modulus of biological cells in AFM indentation experiments, Methods, 60 (2013) 202-213.

[18] F. Gaboriaud, S. Bailet, E. Dague, F. Jorand, Surface structure and nanomechanical properties of *Shewanella putrefaciens* bacteria at two pH values (4 and 10) determined by atomic force microscopy, Journal of Bacteriology, 187 (2005) 3864-3868.

[19] G. Francius, P. Polyakov, J. Merlin, Y. Abe, J.-M. Ghigo, C. Merlin, C. Beloin, J.F.L. Duval, Bacterial surface appendages strongly impact nanomechanical and electrokinetic properties of *Escherichia coli* cells subjected to osmotic stress, PLoS ONE, 6 (2011) e20066.

[20] W. Zhang, A.G. Stack, Y. Chen, Interaction force measurement between *E. coli* cells and nanoparticles immobilized surfaces by using AFM, Colloids and Surfaces B: Biointerfaces, 82 (2011) 316-324.

[21] A. Touhami, M.H. Jericho, J.M. Boyd, T.J. Beveridge, Nanoscale characterization and determination of adhesion forces of *Pseudomonas aeruginosa* pili by using atomic force microscopy, Journal of Bacteriology, 188 (2006) 370-377.

[22] Y. Chen, W. Norde, H.C. van der Mei, H.J. Busscher, Bacterial cell surface deformation under external loading, mBio, 3 (2012).

[23] K.E. Bremmell, A. Evans, C.A. Prestidge, Deformation and nano-rheology of red blood cells: An AFM investigation, Colloids and Surfaces B: Biointerfaces, 50 (2006) 43-48.

[24] M.P. Silverman, D.G. Lundgren, Studies on the chemoautotrophic iron bacterium *Thiobacillus ferrooxidans*: I. An improved medium and a harvesting procedure for securing high cellular yields., Journal of Bacteriology, 77 (1959) 642-647.

[25] B.C. Donose, E. Taran, I.U. Vakarelski, H. Shinto, K. Higashitani, Effects of cleaning procedures of silica wafers on their friction characteristics, Journal of Colloid and Interface Science, 299 (2006) 233-237.
[26] F. Fairbrother, H. Mastin, Studies in electro-endosmosis. Part I., Journal of the Chemical Society, Transactions, 125 (1924) 2319-2330.
[27] D. Fornasiero, V. Eijt, J. Ralston, An electrokinetic study of pyrite oxidation, Colloids and Surfaces, 62 (1992) 63-73.
[28] M. Diao, E. Taran, S. Mahler, T.A.H. Nguyen, A.V. Nguyen, Quantifying adhesion of acidophilic bioleaching bacteria to silica and pyrite by atomic force microscopy with a bacterial probe, Colloids and Surfaces B: Biointerfaces, 115 (2014) 229-236.
[29] Y. Lo, N.D. Huefner, W.S. Chan, P. Dryden, B. Hagenhoff, T.P. Beebe, Organic and Inorganic Contamination on Commercial AFM Cantilevers, Langmuir, 15 (1999) 6522-6526.
[30] X. Sheng, Y.P. Ting, S.O. Pehkonen, Force measurements of bacterial adhesion on metals using a cell probe atomic force microscope, Journal of Colloid and Interface Science, 310 (2007) 661-669.
[31] J.E. Sader, I. Larson, P. Mulvaney, L.R. White, Method for the calibration of atomic force microscope cantilevers, Review of Scientific Instruments, 66 (1995) 3789-3798.
[32] J.N. Israelachvili, Intermolecular and surface forces, Academic Press, London ; New York, 1992.
[33] S.J. O'Shea, M.E. Welland, T. Rayment, An atomic force microscope study of grafted polymers on mica, Langmuir, 9 (1993) 1826-1835.
[34] A. Touhami, B. Nysten, Y.F. Dufrêne, Nanoscale mapping of the elasticity of microbial cells by atomic force microscopy, Langmuir, 19 (2003) 4539-4543.
[35] B. Park, N.I. Abu-Lail, Variations in the nanomechanical properties of virulent and avirulent *Listeria monocytogenes*, Soft Matter, 6 (2010) 3898-3909.
[36] M. Li, L. Liu, N. Xi, Y. Wang, X. Xiao, W. Zhang, Nanoscale imaging and mechanical analysis of Fc receptor-mediated macrophage phagocytosis against cancer cells, Langmuir, 30 (2014) 1609-1621.
[37] K.L. Johnson, I. Books24x, Contact mechanics, Cambridge University Press, New York, 1985.
[38] H. Hertz, On the contact of elastic bodies, Miscellaneous Papers, Macmillan, New York, 1896, pp. 146-162.
[39] M.A. Beckmann, S. Venkataraman, M.J. Doktycz, J.P. Nataro, C.J. Sullivan, J.L. Morrell-Falvey, D.P. Allison, Measuring cell surface elasticity on enteroaggregative *Escherichia coli* wild type and dispersin mutant by AFM, Ultramicroscopy, 106 (2006) 695-702.
[40] X. Li, B.E. Logan, Analysis of bacterial adhesion using a gradient force analysis method and colloid probe atomic force microscopy, Langmuir, 20 (2004) 8817-8822.
[41] Q.S. Li, G.Y.H. Lee, C.N. Ong, C.T. Lim, AFM indentation study of breast cancer cells, Biochemical and Biophysical Research Communications, 374 (2008) 609-613.
[42] J.K. Li, R.M.A. Sullan, S. Zou, Atomic force microscopy force mapping in the study of supported lipid bilayers, Langmuir, 27 (2010) 1308-1313.
[43] P.J. Bujalowski, A.F. Oberhauser, Tracking unfolding and refolding reactions of single proteins using atomic force microscopy methods, Methods, 60 (2013) 151-160.
[44] T.S. Tsapikouni, Y.F. Missirlis, Measuring the force of single protein molecule detachment from surfaces with AFM, Colloids and Surfaces B: Biointerfaces, 75 (2010) 252-259.
[45] C. Bustamante, J.F. Marko, E.D. Siggia, S. Smith, Entropic elasticity of lambda-phage DNA, Science (New York, N.Y.), 265 (1994) 1599-1600.
[46] P.K. Sharma, A. Das, K. Hanumantha Rao, K.S.E. Forssberg, Surface characterization of *Acidithiobacillus ferrooxidans* cells grown under different conditions, Hydrometallurgy, 71 (2003) 285-292.
[47] P. Devasia, K.A. Natarajan, D.N. Sathyanarayana, G.R. Rao, Surface chemistry of *Thiobacillus ferrooxidans* relevant to adhesion on mineral surfaces, Appl. Environ. Microbiol., 59 (1993) 4051-4055.
[48] J. Kiwi, V. Nadtochenko, Evidence for the mechanism of photocatalytic degradation of the bacterial wall membrane at the TiO2 interface by ATR-FTIR and laser kinetic spectroscopy, Langmuir, 21 (2005) 4631-4641.
[49] A. Vilinska, K.H. Rao, Surface characterization of *Acidithiobacillus ferrooxidans* adapted to high copper and zinc ions concentration, Geomicrobiol J, 28 (2011) 221-228.
[50] M. Sletmoen, G. Maurstad, P. Sikorski, B.S. Paulsen, B.T. Stokke, Characterisation of bacterial polysaccharides: steps towards single-molecular studies, Carbohydrate Research, 338 (2003) 2459-2475.
[51] C.-g. Zhang, R.-y. Zhang, J.-l. Xia, Q. Zhang, Z.-y. Nie, Sulfur activation-related extracellular proteins of *Acidithiobacillus ferrooxidans*, Transactions of Nonferrous Metals Society of China, 18 (2008) 1398-1402.
[52] L.S. Dorobantu, S. Bhattacharjee, J.M. Foght, M.R. Gray, Analysis of force interactions between AFM tips and hydrophobic bacteria using DLVO theory, Langmuir, 25 (2009) 6968-6976.
[53] F. Gaboriaud, B.S. Parcha, M.L. Gee, J.A. Holden, R.A. Strugnell, Spatially resolved force spectroscopy of bacterial surfaces using force-volume imaging, Colloids and Surfaces B: Biointerfaces, 62 (2008) 206-213.

584 [54] N.I. Abu-Lail, T.A. Camesano, Role of ionic strength on the relationship of biopolymer conformation,
585 DLVO contributions, and steric interactions to bioadhesion of *Pseudomonas putida* KT2442,
586 Biomacromolecules, 4 (2003) 1000-1012.
587 [55] J. Zhu, Q. Li, W. Jiao, H. Jiang, W. Sand, J. Xia, X. Liu, W. Qin, G. Qiu, Y. Hu, L. Chai, Adhesion forces
588 between cells of *Acidithiobacillus ferrooxidans*, *Acidithiobacillus thiooxidans* or *Leptospirillum ferrooxidans*
589 and chalcopyrite, Colloids and Surfaces B: Biointerfaces, 94 (2012) 95-100.
590 [56] P. Polyakov, C. Soussen, J. Duan, J.F.L. Duval, D. Brie, G. Francius, Automated force volume image
591 processing for biological samples, PLoS ONE, 6 (2011) e18887.
592 [57] H. Wang, J.J. Wilksch, T. Lithgow, R. Strugnell, M.L. Gee, Nanomechanics measurements of live bacteria
593 reveal a mechanism for bacterial cell protection: the polysaccharide capsule in *Klebsiella* is a responsive
594 polymer hydrogel that adapts to osmotic stress, Soft Matter, 9 (2013) 7560-7567.

595

596

597

Captures to Figures

Figure 1. (A) Schematic of the relative positions of a bacterial probe with cell deformation (not to scale). The silica microsphere was omitted for simplification. z_0 is the initial piezo position of the cantilever; z is the relative piezo position of the cantilever; d is the cantilever deflection; δ is the deformation of the cell; s_0 is the initial separation between sample and the substrate surface; s is the actual separation distance between the two surfaces. (B) Schematic illustration of the abbreviations used to calculate the interaction force from the pressure (force per unit area). The cell is considered as a microsphere.

Figure 2. (A) A representative SEM image of a bacterial probe of *A. f* (Fe^{2+}). (B) An AFM height image of *A. f* (Fe^{2+}) immobilized on a glass slide. (C) Typical force curves of ferrous ion-grown cells showing the adhesion events, jump-in events and deformation of the cell.

Figure 3. (A) Zeta potentials of *A. f* and silica wafers under various salt concentrations. (B) FTIR spectra of *A. f* cells cultured with (a) ferrous ions and (b) elemental sulfur.

Figure 4. Histograms of adhesion forces and representative retraction curves (inset) obtained from (A) *A. f* (Fe^{2+}) and (B) *A. f* (S^0) at various salt concentrations. Red lines on retraction curves of sulfur-grown *A. f* show that the adhesion forces are well-fitted by the wormlike chain model described by Eq. (6).

619 **Figure 5.** Scatter plots of the adhesion forces versus snap-off distances measured between the
620 substrates and (A) *A. f* (Fe^{2+}) or (B) *A. f* (S^0). Data points were randomly collected from 30
621 different retraction curves measured for each salt concentration.

622

623 **Figure 6.** Representative approaching curves fitted with steric model showing the effect of
624 ionic strength on approaching curves of (A) *A. f* (Fe^{2+}) and (B) *A. f* (S^0) on the silica surface.
625 Histograms (C and D) of the Young's modulus obtained at various salt concentrations.

626

627 **Figure 7.** Effect of loading forces on the approaching curves of *A. f* (Fe^{2+}) on silica surface in
628 0.001 M KCl solution.

629

629

630 **Captures to Tables**

631 **Table 1.** Effect of salt concentration on the average properties (mean±SE) of adhesion events

632 between bacteria and substrates

633

633 **Table 1.** Effect of salt concentration on the average properties (mean±SE) of adhesion events

634 between bacteria and substrates

Bacteria	Substrates	Salt conc. (M)	Adhesion events (%)	Mean adhesion force (nN)	Stair-step unfolding force (nN)	Snap-off distance (nm)	
						Mean	Range
A. f (Fe^{2+})	Silica	0.001	16	0.057±0.017	0.041±0.007	1498±332	308~2187
		0.01	28	0.074±0.023	0.065±0.016	558±275	40~1644
		0.1	42	0.026±0.013	0.048±0.005	254±62	78~627
		1	47	0.088±0.021	0.091±0.015	611±184	131~1679
	Pyrite	0.001	22	0.044±0.018	0.038±0.007	611±221	33~1625
		0.01	29	0.057±0.022	0.066±0.012	747±302	211~1983
		0.1	100	0.085±0.031	0.081±0.075	942±198	89~1840
		1	22	0.061±0.026	0.089±0.036	536±220	237~1853
A. f (S^0)	Silica	0.001	48	0.211±0.117	NA	267±36	76~401
		0.01	100	0.352±0.075	NA	222±44	58~351
		0.1	86	0.287±0.084	NA	326±102	73~800
		1	72	0.113±0.076	NA	537±176	102~1024
	Pyrite	0.001	53	0.069±0.036	NA	260±93	46~625
		0.01	75	0.053±0.021	NA	409±130	92~1154
		0.1	100	0.081±0.024	NA	572±182	34~1042
		1	86	0.082±0.035	NA	499±251	32~1688

635 NA: value was not estimated from this study.

636

636

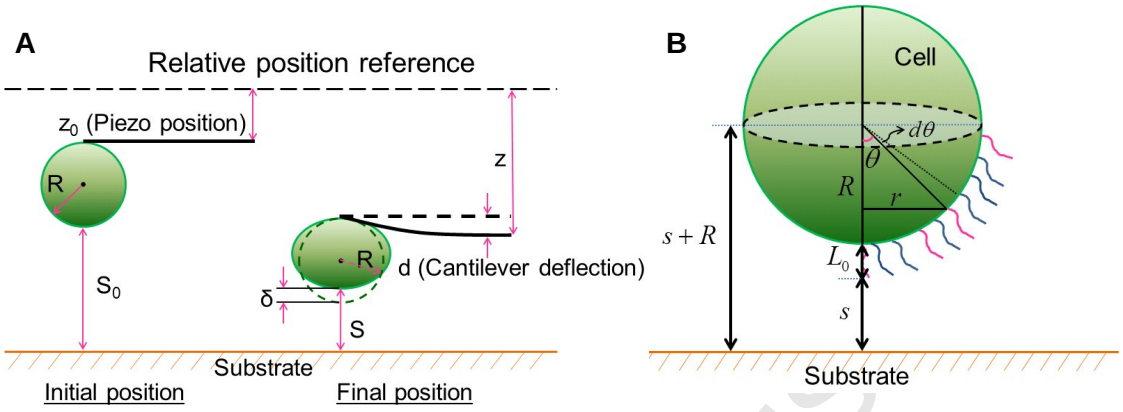

637

638 **Figure 1.** (A) Schematic of the relative positions of a bacterial probe with cell deformation
639 (not to scale). The silica microsphere was omitted for simplification. z_0 is the initial piezo
640 position of the cantilever; z is the relative piezo position of the cantilever; d is the cantilever
641 deflection; δ is the deformation of the cell; s_0 is the initial separation between sample and
642 the substrate surface; s is the actual separation distance between the two surfaces. (B)
643 Schematic illustration of the abbreviations used to calculate the interaction force from the
644 pressure (force per unit area). The cell is considered as a microsphere.

645

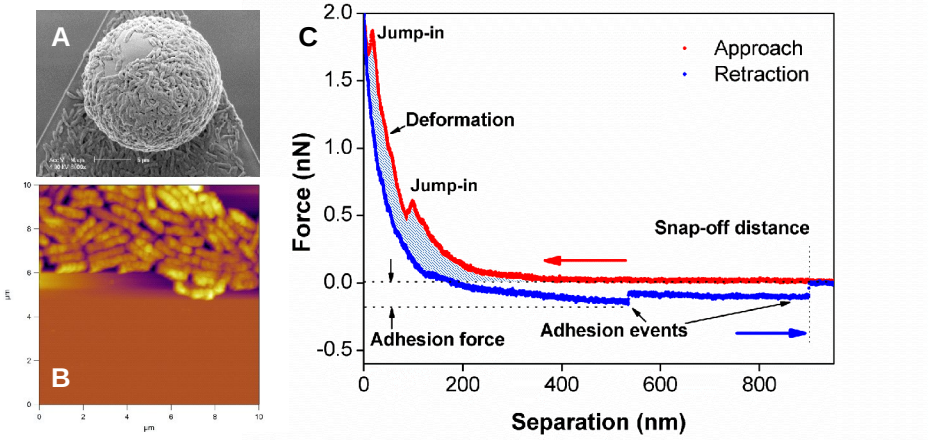

Figure 2. (A) A representative SEM image of a bacterial probe of *A. f* (Fe^{2+}). (B) An AFM height image of *A. f* (Fe^{2+}) immobilized on a glass slide. (C) Typical force curves of ferrous ion-grown cells showing the adhesion events, jump-in events and deformation of the cell.

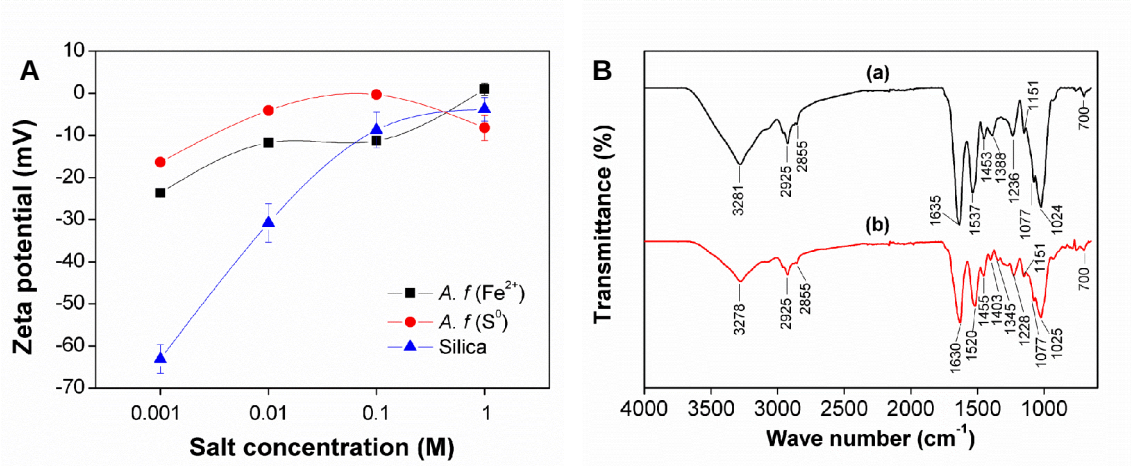

Figure 3. (A) Zeta potentials of *A. f* and silica wafers under various salt concentrations. (B) FTIR spectra of *A. f* cells cultured with (a) ferrous ions and (b) elemental sulfur.

655

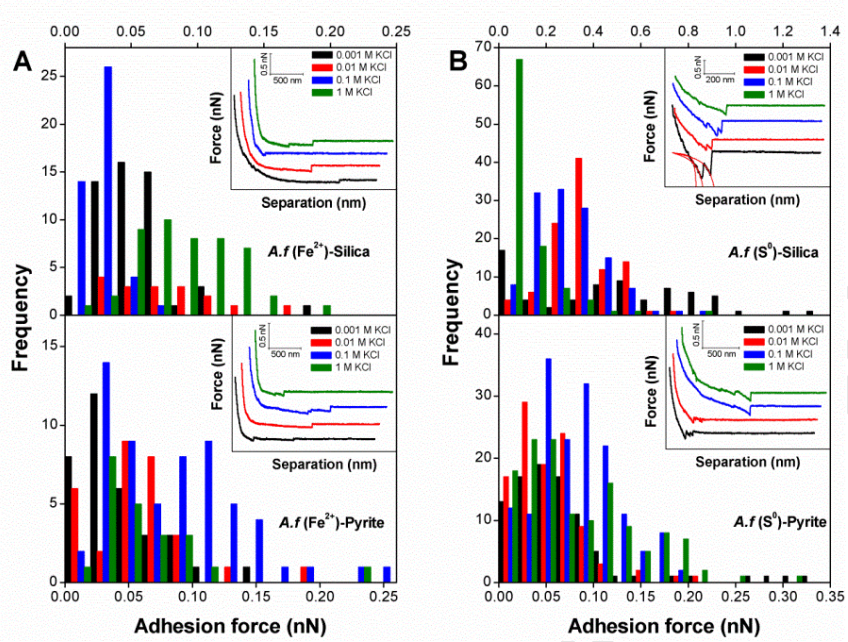

656

657 **Figure 4.** Histograms of adhesion forces and representative retraction curves (inset) obtained
658 from (A) *A. f* (Fe^{2+}) and (B) *A. f* (S^0) at various salt concentrations. Red lines on retraction
659 curves of sulfur-grown *A. f* show that the adhesion forces are well-fitted by the wormlike
660 chain model described by Eq. (6).

661

661

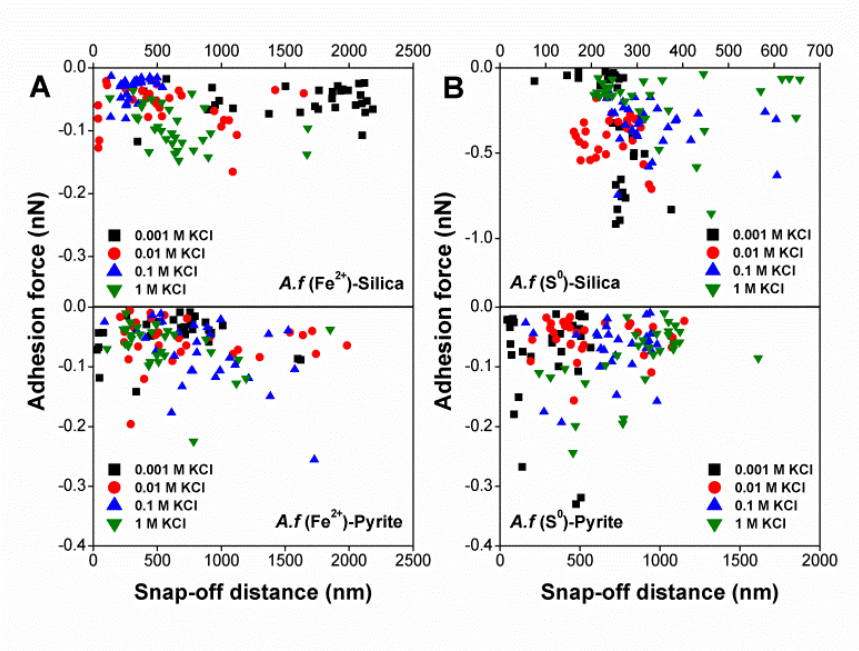

662

663 **Figure 5.** Scatter plots of the adhesion forces versus snap-off distances measured between the
664 substrates and (A) *A. f* (Fe^{2+}) or (B) *A. f* (S^0). Data points were randomly collected from 30
665 different retraction curves measured for each salt concentration.

666

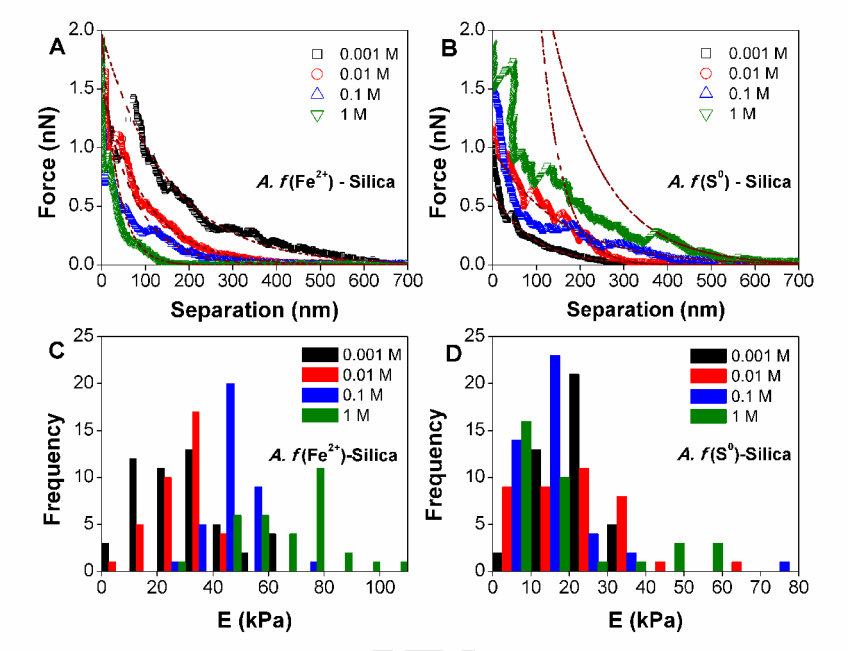

Figure 6. Representative approaching curves fitted with steric model showing the effect of ionic strength on approaching curves of (A) *A. f* (Fe^{2+}) and (B) *A. f* (S^0) on the silica surface. Histograms (C and D) of the Young's modulus obtained at various salt concentrations.

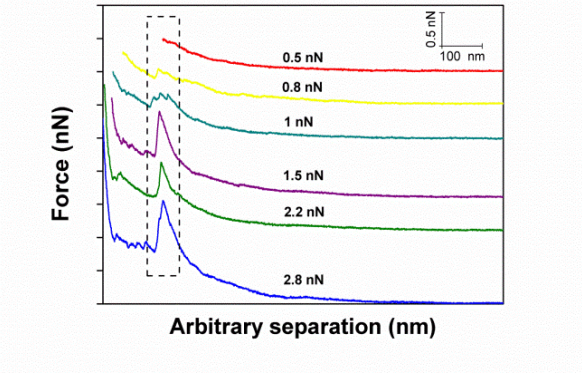

674 **Figure 7.** Effect of loading forces on the approaching curves of *A. f* (Fe^{2+}) on silica surface in

675 0.001 M KCl solution.

676